Brain Nerve Bundles Estimation by Restoring and Filtering Intra–Voxel Information in Diffusion Tensor MRI

Alonso Ramírez-Manzanares and Mariano Rivera
Centro de Investigacion en Matematicas A.C.,
Apdo. Postal 402, Guanajuato, Gto., 36000, Mexico
{alram, mrivera}@cimat.mx

Abstract

We present a regularized method for solving an inverse problem in Diffusion Tensor Magnetic Resonance Imaging (DT–MRI) data. In the case of brain images, DT–MR obtains a tensor field that indicates the local orientation of nerve bundles. Now days, the spatial resolution of this technique is limited by the partial volume effect; i.e. the measured tensors at voxels that contain fiber crossings or bifurcations results from the addition of several tensors, each one oriented with its corresponding nerve bundle. In this paper, we proposed a method for recovering the original intra–voxel information. We assume that the observed tensors are a linear combination of a given tensor base, therefore, the aim of our approach is the computation of the unknown coefficients of this linear combination. By regularizing the problem, we introduce the prior information about the piecewise smoothness of nerve bundles orientation. Such regularization process performs an anisotropic filtering of the coefficients. As a result, we recover a multi–tensor field. Moreover, we propose to estimate the nerve bundles trajectory by performing stochastic walks of particles in the computed multi–tensor field. In order to demonstrate the performance of the method, we ran several experiments using both synthetic and real data.

1 Introduction

One of the most challenger medical goals is the estimation of brain connectivity in vivo. For this purpose, a special Resonance Magnetic Imaging (MRI) technique named Diffusion Tensor Magnetic Resonance Imaging (DT–MRI) is used. The 3–dimensional (3D) Diffusion Tensor Image (DTI), measures the microscopic diffusion of water in a tissue, such diffusion is constrained by the direction of nerve bundles. For a given voxel r, the Stejskal–Tanner equation[1],

$$S_r = S_{0r} \exp(-b\mathbf{g}^T \mathbf{D}_r \mathbf{g}), \tag{1}$$

shows the relationship between the signal magnitude measured without diffusion, S_0, and the one attenuated by the water diffusion in the tissue, S. The unitary vector $\mathbf{g} = [g_x, g_y, g_z]^T$ indicates the direction in which a directional independent magnetic gradient is applied, $\mathbf{D}_r$ is a positive definite symmetric tensor and b is a constant that depends on the acquisition parameters, see [1] for more details. The conventional procedure for computing the tensor field $\mathbf{D}$, at each voxel r, is based on a least–squares method: at least 8 diffusion images (each one corresponding to a magnetic gradient) are taken and then the least–squares problem for the 6+1 unknowns is solved [2]. These unknowns are the six independent components of the symmetric diffusion tensor $\mathbf{D}_r$, and S_{0r}.

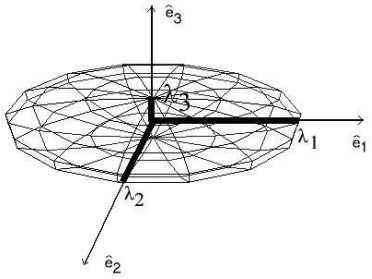

Figure 1: Geometric interpretation of the diffusion tensor.

The diffusion tensor can be visualized as a 3D ellipsoid, as shown in Figure 1. In this geometric interpretation, the principal axis are aligned according to the eigenvectors $[\hat{e}_1, \hat{e}_2, \hat{e}_3]$, and the eigenvalues $\lambda_1 \geq \lambda_2 \geq \lambda_3$, define the diffusion magnitude along each axis. Thus, $\hat{e}_1$ is named the principal diffusion direction (PDD). A study of the behavior of the eigenvalues gives more insight of the angular variation of the diffusion into the voxels. Three geometric classes of diffusion based on the relationship between the eigenvalues are discussed in [2], they are:

1. LINEAR: $\lambda_1 \gg \lambda_2 \simeq \lambda_3$, high anisotropy . The geometric interpretation of such tensor has a cigarette shape.
2. PLANAR: $\lambda_1 \simeq \lambda_2 \gg \lambda_3$, medium anisotropy. The geometric interpretation of the tensor looks like a plate.
3. SPHERICAL: $\lambda_1 \simeq \lambda_2 \simeq \lambda_3$, low anisotropy. This case can be visualized as a soccer ball.

In the 3D case, the one that concerns here, the measure of anisotropy most commonly used is the *fractional anisotropy*

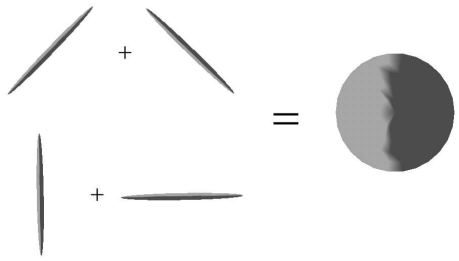

Figure 2: Two pairs of high–anisotropic tensors which addition produces the same low–anisotropic tensor

(FA) [3, 4]:

$$FA(\mathbf{D}) = \sqrt{\frac{(\lambda_1 - \lambda_2)^2 + (\lambda_1 - \lambda_3)^2 + (\lambda_2 - \lambda_3)^2}{2\,(\lambda_1^2 + \lambda_2^2 + \lambda_3^2)}}, \quad (2)$$

where λ_k is the k^{th} eigenvector of $\mathbf{D}$. Note that for highly anisotropic tensors, FA is close to one, while FA is close to zero for a low anisotropic tensor (the spherical case).

In addition to standard studies on MR images, as the classification of voxels between white/gray matter tissues, DT–MR images provide tissue information according to the FA. However, perhaps, the most important information that can be inferred from DT–MR images is tissue connections. That means that for brain DT–MR images, one could estimate axons bundle pathways by following the PDD's in regions with high anisotropy (sites where FA takes large values). This information is very useful in medical image research, due to the relationship of brain connectivity with several diseases, and in general, with brain development.

Like any other imaging acquisition technique, the information accurateness is corrupted by noise, so that, a filtering process is required. Other problem on DT–MR images concerns the limited resolution for dealing with partial volume voxels. That is, when a voxel contains a cross or a bifurcation of fibers.

1.1 Statement of the Problem

Noise is not the only problem precluding DT–MR images. Partial volume voxels have a more pernicious effect than in standard MR images: the observed diffusion tensor at voxels where two or more fibers cross, split, or merge, is the addition of several diffusion tensors,—each one aligned with a particular bundle fiber. Tensor addition is very different to vector addition. The addition of two almost orthogonal tensors with high–anisotropy results in a tensor with low–anisotropy. This fact increases the uncertainty of the tissue orientation and reduces the anisotropy of the observed tensor [1]. Furthermore, the inverse problem is not well–defined: different combinations of high–anisotropic tensors may results in the same low–anisotropic tensor, see Figure 2. So, one needs to solve these two issues in order to recover the two tensors that produced the measured tensor.

If the spatial image resolution is increased, then the partial volume effect could be diminished at those voxels at the boundary of differently oriented tissues, but with a significant increment in the acquisition time. However, the partial volume effect produced by fiber crossing can not be diminished by increasing the spatial resolution. Therefore, in order to compute a good estimation of the original fiber pathways, it is necessary to develop a process that recover the lost intra–voxel information.

Several methods are reported in the literature for estimating fiber pathways. Those methods are based on: performing deterministic walks of particles on the tensor field by following the PDD [4, 17], or by propagating a wavefront with the use of the fast marching method [14]. In [6], the displacement direction of the particle is computed with a deterministic method. Then, this direction is randomly disturbed in order to introduce a stochastic behavior. Anyway, the partial volume effect reduces the accurateness of the estimated fiber pathways. Figure 3 illustrates the case of estimating fiber pathways in a fiber crossing. One can see in this figure that the intersection of two bundle fibers with high fractional anisotropy (FA close to 1), produces a region where the local orientation information is uncertain (with FA close to 0). To ensure the correct particle trajectory through the fiber crossing, these particles should reach the low confident region with a trajectory aligned to the tracked fiber. Otherwise, the particle trajectory could be bent. In [1, 2, 6], an homogeneous Gaussian smoothing is applied to the tensor field. Although the blurring produces a denoising effect, it also increases the uncertainty in the orientation. Another approach [17], aims to reduce the uncertainty in the direction by computing the displacement of each particle with a direction computed from a robust anisotropic average of the tensors in a neighborhood around the particle. More recently, Tuch et al. [9, 10, 11], proposed a high angular resolution imaging method based on an observation model built by a finite mixture of Gaussians:

$$S_r = S_{0r} \sum_j f_i \exp(-b\mathbf{g}^T \mathbf{D}_{ir} \mathbf{g}), \quad (3)$$

where f_i is the contribution of the tensor $\mathbf{D}_i$ to the total diffusion in the voxel. Both, f and $\mathbf{D}_i$, are vector and tensor unknown fields, respectively, that are computed, independently for each voxel, from a large set of acquired images $\{S\}$. This Diffusion Multi–Tensor Magnetic Resonance Imaging (DMT–MRI) technique allows one to recover the intra–voxel information that is not observed in the standard DT–MRI. This imaging method is considered the state of the art in DT–MRI. The drawbacks of the method, are: the large number of additional diffusion images $\{S\}$ required (for instance, in [11], 126 diffusion 3D–images are used), the consequent increment on their acquisition time, and the algorithmic problems related to Equation (3) which is highly nonlinear, so that multiple restarts of the optimization method are required to prevent the algorithm from settling in a local minima. Furthermore, no stable solution has been reported for more than 2 fiber bundles, i.e. for $j > 2$ (see discussion on Ref. [11], Chap. 7).

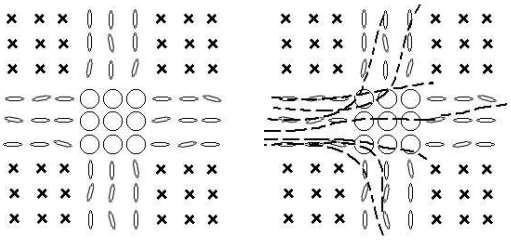

a) b)

Figure 3: Left: A tensor field on a fiber crossing. Right: particles walking through the horizontal fiber path; most particles are deviated from the right trajectory, due to the uncertain direction on the cross.

The method we propose here, consist of two stages: i) restoration of the intra–voxel information by computing the coefficients of a tensor basis field, and ii) estimation of fiber pathways by particle stochastic walks. The method for reconstruction of the intra–voxel information uses standard DT–MR images as input data. That means that the existing large data base or new measurements of DT–MR images can be processed at a fraction of the acquisition time with respect to DMT–MR images. Additionally, the proposed method is based on the minimization of a quadratic cost function that can be efficiently minimized with standard deterministic algorithms, in particular we used an iterated Gauss–Seidel scheme. In the second stage, we estimate bundle fibers by means of a stochastic walk procedure. This stochastic walk is formulated in a Bayessian framework where the new position of the particle is computed by sampling the posterior distribution of displacement directions. In order to compute this posterior distribution, we take into account: the last positions of the particle in a likelihood term (actually, we investigate Markovian process models of first or second order), and a prior (regularization) term that codifies the information of the reconstructed diffusion multi–tensor field.

The structure of this paper is as follows. In Section 2, we present the proposed restoration method for the intra–voxel structure information and the algorithmic details for minimizing the proposed cost function. In order to estimate axons bundle pathways, we proposed in Section 3 a stochastic walk method that uses the restored multi–tensor field. Section 4 describes experiments with both synthetic and real DT–MR images. Finally, our conclusions are given in Section 5.

2 Restoration of Intra–Voxel Information

This section introduces the first stage of the method: the procedure for recovering the intra–voxel structure. In order to motivate our approach, we first present the observation model of the measured diffusion tensor field.

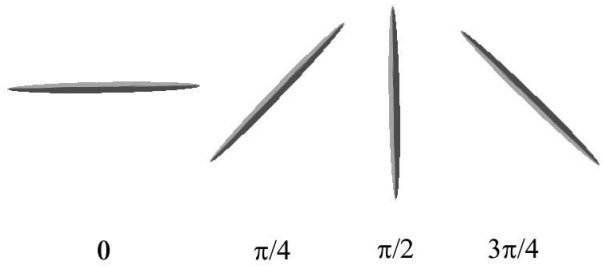

Figure 4: A example of 2D tensor base set $\bar{\mathbf{T}}$, with cardinality equal to four.

2.1 Observation Model of the Diffusion tensor

Differently to the method reported by Tuch et. al. [see model (3)], we do not use as input data the raw data set $\{S\}$ [as in model (3)], but the measured (observed) tensor field $\mathbf{D}$. We assume that observed tensor $\mathbf{D}_r$, at the voxel r, is the result of a summation of individual tensors $\mathbf{T}$, such tensors correspond with no–collinear fibers into the voxel, this is:

$$\mathbf{D}_r = \sum_{i}^{M_r} \mathbf{T}_{ir} + \eta_r. \tag{4}$$

where M_r is equal to the number of fibers with a different orientation (note that M depends on the voxel), the tensor η represents the independent additive noise. The solution to the inverse problem implicit in the model (4), involves the computation of the tensors $\{\mathbf{T}_{ir}\}$, with arbitrary size and orientation. Instead of the "exact" model (4), we propose to use an approached model based on a predefined tensor basis, $\bar{\mathbf{T}}$. The base tensors are chosen such that they are uniformly distributed on 3D space of orientations, and have $\mathrm{FA}(\bar{\mathbf{T}}_i) \approx 1$ (Figure 4 shows a 2D example of a basis set of four tensors with their orientations uniformly distributed in the interval $[0, 2\pi]$). Therefore, the approximated observation model is [compare with (3) and (4)]:

$$\mathbf{D}_r = \sum_{i}^{N} \alpha_{ir} \bar{\mathbf{T}}_i + \eta_r. \tag{5}$$

where N is the cardinality of the base $\bar{\mathbf{T}} = [\bar{\mathbf{T}}_1, \bar{\mathbf{T}}_2, ..., \bar{\mathbf{T}}_i, ..., \bar{\mathbf{T}}_N]$ and $\alpha = [\alpha_1, \alpha_2, ..., \alpha_i, ..., \alpha_N]^T$ is a vector field such that the scalar α_{ir} denotes the contribution of the individual base tensor $\bar{\mathbf{T}}_i$ at the voxel r to the observed tensor $\mathbf{D}_r$. For a tensor basis with high angular resolution (N is relatively large), one can expect that in a voxel where there is only one fiber path, a single coefficient α_i will take a significant large value and the others $\alpha_{j\neq i}$ would take values close to zero. In the same way, if there are *m* different fiber paths in a voxel, then we expect that *m* coefficients α_k will take a significant large value with respect to the other coefficients.

2.2 Cost Function for Restoring Intra–Voxel DT–MRI Structure

Model (5) can represent more than one tensor in a voxel, but, it is still necessary to determine which linear combina-

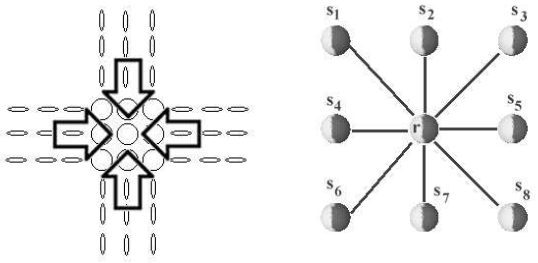

a) b)

Figure 5: a) Information propagation from the anisotropic to isotropic regions. b) A 2D neighborhood $\mathcal{N}_r$ of the voxel r.

tion of base tensors, in $\bar{\mathbf{T}}$, best fit the data $\mathbf{D}_r$. Unfortunately, the computation of the positive coefficients, $\{\alpha_{ir}\}$, is an ill–posed problem because the information provided by the observed tensor, $\mathbf{D}_r$, and the model (5) are not enough for computing an unique solution. So that, we regularize the problem by using the voxel spatial context information. Therefore, the coefficient information should be propagated from regions with high anisotropy to those with low anisotropy. This is consistent with prior knowledge that fiber crossing occurs in regions with low anisotropy, this is illustrated in Figure 5a. To solve this problem, we propose to minimize a cost function of the form:

$$\hat{U}(\alpha) = \sum_r U(\alpha; r). \tag{6}$$

This global cost $\hat{U}$ is the summation of the individuals cost functions $U(\alpha; r)$ associated to each voxel, r. A preliminary version of the local cost function that it codifies the above expressed is:

$$\begin{aligned} U(\alpha; r) &= \omega_r \rho_1 \left(\sum_i \alpha_{ir} \bar{\mathbf{T}}_i, \mathbf{D}_r \right) \\ &\quad + \lambda_s \sum_{s \in \mathcal{N}_r} \rho_2(\alpha_r, \alpha_s) + \lambda_c \rho_3(\alpha_r), \end{aligned} \tag{7}$$

where, in general, the potential function ρ_j (with $i = 1, 2, 3$) defines a norm. Now, we clarify the meaning of each term in (7):

1. In the Bayessian regularization framework [12, 13], the first term corresponds to the negative log–likelihood and penalizes the difference between the proposed model and the observed tensor $\mathbf{D}_r$. In this particular case, we choose the Frobenius's norm for quantifying such difference. In order to promote the propagation of information of coefficients from the regions with high anisotropy to those regions with low anisotropy, and to restrict the opposite, we weight the data term with the *fractional anisotropy* of the data: $\omega_r = FA(\mathbf{D}_r)$, see Eq. (2).

2. The second term (first regularization term) codifies the prior knowledge by penalizing the spatial inhomogeneity of the vector α. The relative contribution of this term, to the total cost, is controlled by the parameter λ_s. $\mathcal{N}_r$ is the set of neighbors voxels of r (a second order neighborhood system), see Figure 5b. We want to constraint this smoothness process to be performed along the fiber bundle. This is achieved by an anisotropic filtering of the coefficients α. Therefore, we use the tensor $\bar{\mathbf{T}}_i$ as the inertia tensor for controlling such anisotropic filtering. Thus, ρ_2 is a weighted quadratic potential of the first differences: $\alpha_r - \alpha_s$. In Ref. [8] is proposed a method for compute these weights given an inertia tensor. In our formulation, these weights are computed as follows:

$$w_{irs} = \frac{(s-r)^T \bar{\mathbf{T}}_{ir} (s-r)}{\|s-r\|^4}. \tag{8}$$

where w_{irs} is the weight associated with the potential: $(\alpha_{ir} - \alpha_{is})^2$.

3. The third term, controlled by the parameter λ_c, promotes large contrast in the α_{ir} coefficients. Figure 6a shows a low contrast example, with high uncertainty about discerning which tensors are more representative. On the other hand, Figure 6b shows an example with low uncertainty; only two coefficients have large values and the others are close to zero. Also, Figure 6 suggests a method for improving the contrast: by forcing each α_{ir} coefficient to be different from the arithmetic mean: $\bar{\alpha}_r = \sum_i \alpha_{ir}/N$.

Already we have all the ingredients for the final energy function, the complete local energy function is:

$$\begin{aligned} U(\alpha, r) &= \omega_r \sum_j \left(\sum_i \alpha_{ir} \bar{T}_{ij} - D_{rj} \right)^2 \\ &\quad + \lambda_s \sum_{s:s \in \mathcal{N}_r} \sum_i w_{irs} (\alpha_{ir} - \alpha_{is})^2 \\ &\quad - \lambda_c \sum_i (\alpha_{ir} - \bar{\alpha}_r)^2 \end{aligned} \tag{9}$$

with the additional constraint:

$$\alpha_{ir} \geq 0, \forall i, \tag{10}$$

where $i = 1, ..., N$, $j = 1, 2, ..., 9$ is an index that runs over the matrix coefficients, the weights ω_r and w_{irs} are computed with (2) and (8), respectively.

2.3 Minimization Algorithm

The minimization of Eq. (6) is achieved by solving the linear system [given that (9) is quadratic] that results from

$$\frac{\partial U(\alpha, r)}{\partial \alpha_{kr}} = 0. \tag{11}$$

We use a simple Gauss–Seidel scheme, with the additional advantage of low memory requirements, for solving this linear system.

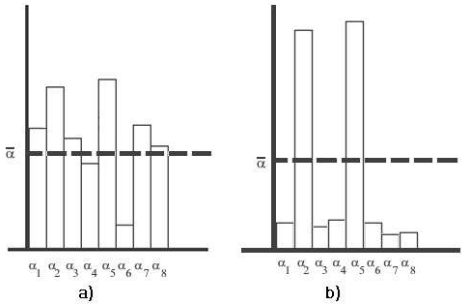

Figure 6: a) Coefficients with low contrast: high uncertainty about the significance of the basis tensors. b) High contrasted coefficients: low uncertainty (see text).

The constraint of positivity on α_{ir}, is satisfied by projecting to zero the negative values in each iteration. According to our experiments, it is important to set the parameter $\lambda_c = 0$, then, once the algorithm has converged (with a low contrast on the α_r vectors) one refines the solution with the right value for λ_c.

3 Stochastic Walks for Estimating Fiber Pathways

The second stage of the method for recovering fiber pathways in DT–MRI, is the computation of walks of virtual particles that move through the computed multi–tensor field. In opposition to deterministic walk methods reported in Refs. [4, 17], our approach is based on stochastic walks. The particles pathways are close related with the fiber structure in the following way: in voxels where only one fiber is present, only one coefficient of the tensor basis field took a significant value and its PDD indicates the fiber orientation. On the other hand, in a bifurcation, two coefficients took a significant value and the particle will choose any of those paths corresponding to the PDD's.

Before we present the stochastic walk method, we will establish some definitions. We denote by $\mathbf{x}_t$ the position vector of the particle at iteration t, then d^*_{t+1} is the unitary vector that leads the particle from the position $\mathbf{x}_t$ to the next step, $\mathbf{x}_{t+1}$, then:

$$\mathbf{x}_{t+1} = \mathbf{x}_t + \delta d^*_{t+1} \tag{12}$$

where δ is the step size.

3.1 Computation of the Displacement Vector

For the computation of the displacement vector, d^*_{t+1} in (12), we use a Bayessian estimation based on a Markov process. This is explained next.

Let $\mathbf{q} = \{q_1, q_2, ..., q_N\}$ be the set of orientations corresponding to the PDD of the base tensors in $\bar{\mathbf{T}}$. Then, by using the Bayes Rule, we compute the probability of choosing a particular q_i orientation, as the orientation of the vector d_{t+1}, given the sequence of displacements $\{d^*_k\}$ (for $k = 1, 2, 3, ...t$) with:

$$P\left(d_{t+1} \parallel q_i \middle| \tilde{d}_t\right) = \frac{1}{Z} P\left(\tilde{d}_t \middle| d_{t+1} \parallel q_i\right) P\left(d_{t+1} \parallel q_i\right) \tag{13}$$

where Z is a normalization constant, $x \parallel y$ denotes that x is parallel to y and the vector $\tilde{d}_t$ is the extrapolated direction estimated from the sequence $\{d^*_k\}$.

The prior probability of a particular orientation, $P\left(d_{t+1} \parallel q_i\right)$, is directly computed from the α's coefficients at position $\mathbf{x}_t$:

$$P\left(d_{t+1} \parallel q_i\right) = \frac{\alpha_{i\mathbf{x}_t}}{\sum_j^N \alpha_{j\mathbf{x}_t}}, \tag{14}$$

where $\alpha_{i\mathbf{x}_t}$ coefficients are computed with a trilinear interpolation because $\mathbf{x}_t \in \Omega \subset \mathbb{R}^3$.

The likelihood term in (13), $P\left(\tilde{d}_t \middle| d_{t+1} \parallel q_i\right)$, is the probability of coming from the direction $\tilde{d}_t$ given that the next direction, d_{t+1}, is parallel to q_i. To compute this likelihood, we need to compute the intersection distance of the projection of the vector $\tilde{d}_t$ with the level curve of $\mathbf{y}^T \bar{\mathbf{T}}_i \mathbf{y} = 1$. Note that $\bar{\mathbf{T}}_i$ is positive definite, and this level curve corresponds to a 3D–ellipsoid. This process is illustrated by Figure 7: the distance from the center to the ellipsoid in the direction $\tilde{d}_t$ is measured for the base tensors corresponding to Figure 4. In this way it is clear that the largest value is computed with the tensor B. Consequently, in this case, it is more likely that the last travel direction of the particle is $\tilde{d}_t$ if the next walk direction is parallel to the PDD of the base tensor B. Thus, to compute the likelihood we use:

$$P\left(\tilde{d}_t \middle| d_{t+1} \parallel q_i\right) = \frac{1}{Z_l} \frac{1}{\sqrt{\tilde{d}_t^T \bar{\mathbf{T}}_i \tilde{d}_t}}. \tag{15}$$

where Z_l is a normalization constant.

Now, in order to compute $\tilde{d}_t$, we do not require the full sequence $\{d^*_k\}$, but only the last ones: d^*_t and d^*_{t-1}. We investigate two cases: to preserve the last tendency or to preserve the last curvature (see Figure 8). These cases are:

1. First Order Walk. Only the previous direction is taken into account for compute $\tilde{d}_t$, we use the model:

$$\tilde{d}_t - d^*_t = 0. \tag{16}$$

In this case, we have $\tilde{d}_t = d^*_t$, and the likelihood term $P\left(d^*_t \middle| d_{t+1} \parallel q_i\right)$ corresponds to a Markov process of first order.

2. Second Order Walk. In order to preserve the curvature of the trajectory, $\tilde{d}_t$ is computed with the model:

$$-\tilde{d}_t + 2d^*_t - d^*_{t-1} = 0. \tag{17}$$

So that, the likelihood takes the form $P\left(d^*_t, d^*_{t-1} \middle| d_{t+1} \parallel q_i\right)$, and it is a second order Markov process.

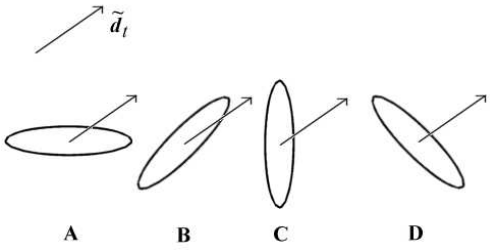

Figure 7: Calculation of the term $P\left(\tilde{d}_t \middle| d_{t+1} \parallel q_i\right)$.

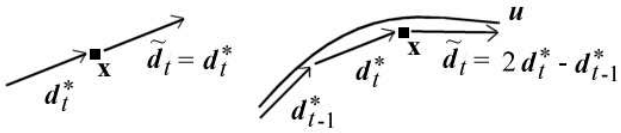

Figure 8: a) Vector $\tilde{d}_t$ for the first order walk. b) Vector $\tilde{d}_t$ for the second order walk.

Finally, the vector d_{t+1}^* is computed by performing a sampling of the posterior probability distribution $P\left(d_{t+1} \parallel q_i \middle| \tilde{d}_t\right)$ (this can be understood as a stochastic tournament), see Eq. (13). The ambiguity in the sign of the orientation is solved by choosing among d_{t+1} and $-d_{t+1}$, the one that the inner product with $\tilde{d}_t$ is positive, i.e. the closest direction with the past trajectory.

3.2 Implementation Details

We scale the step size, δ, with *a priori* probability $P\left(d_{t+1}^* \parallel q_i\right)$ [see Eq. (14)]. Given that the computed walk have coarse trajectories because of the discrete nature of the tensor basis, we refine the vector d_{t+1}^*. Such refinement consists on to use as displacement vector the resultant sum of two vectors: the previous direction step d_t^*, and the winner of the stochastic tournament. In this way, smoother trajectories are obtained. Note that, the refined orientation does not necessary belongs to the set $\mathbf{q}$.

4 Experiments

In this section, we demonstrate the performance of the method by numerical experiments in both synthetic and real DT–MR data. Figure 9 shows the results of the first experiment in synthetic two–dimensional (2D) data. Panel 9a shows the noisy tensor field with a fiber crossing. The restored multi–tensor field is shown in panel 9b. Note that, the right two base tensors are recovered at the intersection and the noise is practically eliminated. Thus, the intra–voxel structure is discovered. Only the base tensors with the α_i coefficients that represent the 95% of the linear combination are displayed. The parameters of the method are $N = 6$, $\lambda_s = 1.0$, $\lambda_c = 0.1$. We choose the base tensors such that their eigen–values are $[\lambda_1, \lambda_2] = [1, 0.1]$.

The second experiment was performed on the 3D synthetic data shown in Figure 10, panel (a). In this case, the tensors show smooth wavy paths and their intersection is not orthogonal. Panel 10b shows the recovered multi–tensor field and panel 10c shows the detail of the intersection. Panel 10d shows the particle paths of a set of 100 particles with starting point in the left part of the horizontal fiber. We note that approximately the 15% of the particles are deviated to the other simulated fiber bundle. This feature is product of the stochastic nature of the particle walks and allows us to explore possible bifurcations in fiber bundles. In comparison, deterministic walk methods will recover the same trajectory for all the particles that where started at the same point. The parameters of the method are: the orientation space is uniformly sampled in 57 orientation ($N = 57$), $\lambda_s = 0.05$, and $\lambda_c = 0.07$. The image dimensions are $32 \times 32 \times 32$ voxels. In this case, we choose the base tensors, such that their eigen–values are $[\lambda_1, \lambda_2, \lambda_3] = [1, 0.1, 0.1]$. We select this tensor basis based on the *prior* knowledge that diffusion along the fiber PDD is about 10 times that of the transversal directions in real axon fibers [18].

Figures 11 and 12 show the results of an experiment with real DT–MRI data. The original DT–MRI data were acquired with a resolution of $128 \times 128 \times 20$, and each voxel corresponds to a volumetric space of $2mm \times 2mm \times 4mm$. We interpolate the data so that each interpolated voxel have a dimension of $1mm \times 1mm \times 1mm$ (it corresponds to $186 \times 154 \times 60$ voxels in the region of interest, i.e. the parallelogram that contains brain tissue). We used the DT data approximation method reported in Ref. [15], with a scaling factor $\Delta = 0.5$. Figure 11a shows the *fractional anisotropy* of an axial slice of the interpolated data and the small square indicate the region of detail. Figure 11b shows the region of detail of the interpolated DT used as input in the algorithm for recovering intra–voxel structure. Figure 11c shows, the detail of the recovered multi–tensor field and Figure 11d the computed trajectories of the particles. In this case, the displacement of the particles was constrained to lay in the axial slice shown in 11a. Figure 12 shows the full view of several pathways computed in the mentioned slice. It was not needed to adjust the parameters for this experiment, the set of parameters and the tensor basis are the same than the used in the experiment of Figure 10. In all the previous experiments, we performed a second order stochastic walks and the step size was $\delta = 0.5P(d_i^*)$.

Finally, figure 13 shows the result of the experiment designed to demonstrate the capability of the method for filtering tensor fields. Panel 13a shows a region of DT–MRI input data, panel 13b shows the the recovered multi–tensor field and panel 13c shows the tensor field computed as the linear combination of the base tensor weighted by the α's coefficients, i.e. with the direct model (5) but without the noise component. Note that the restored tensor field is congruent with the input data and the enhancement is evident: the restoration have more defined local orientations and a higher anisotropy.

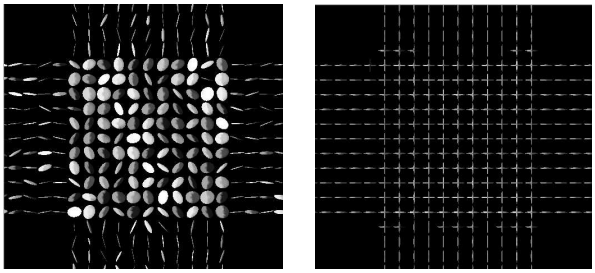

a) b)

Figure 9: A 2D fiber crossing synthetic experiment. In a) noise corrupted 2D tensor field with a fiber crossing. In b) the 2D recovered multi–tensor field.

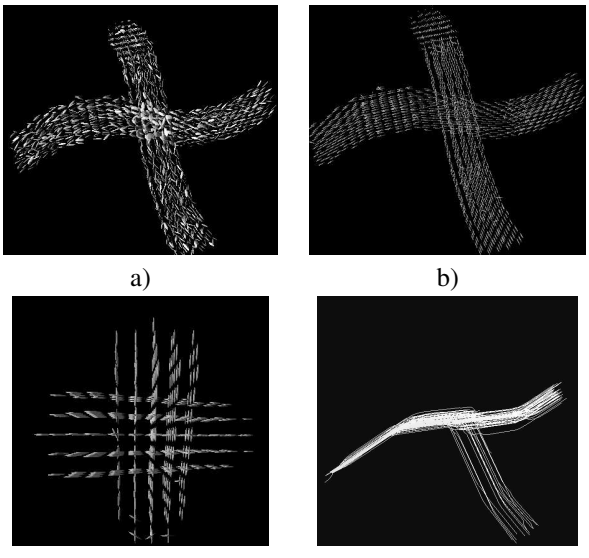

a) b)

c) d)

Figure 10: Results of the numerical experiment with synthetic data (see text).

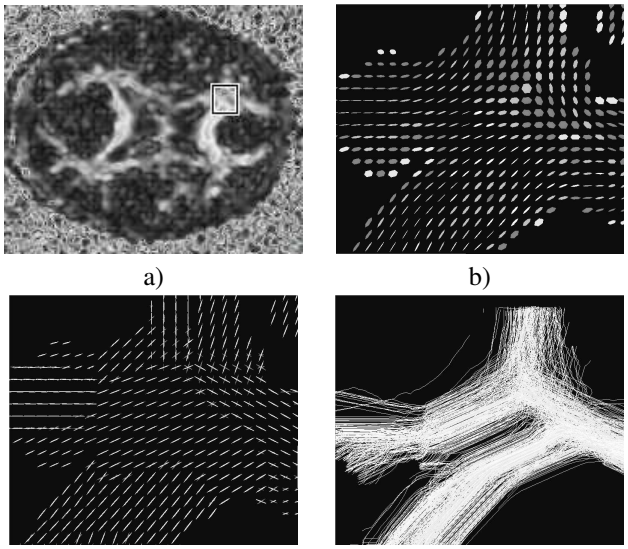

a) b)

c) d)

Figure 11: Results of the numerical experiment with standard DT–MRI data (see text).

Figure 12: particle trajectories computed with the stochastic walk in the recovered multi–tensor field.

5 Conclusions

The main contribution of the paper are the followings:

1. We presented a method that improves the resolution of standard DT–MRI technique and allows one to reconstruct the intra–voxel information as fiber crossing and bifurcations. Therefore, we estimate the intra–voxel information from standard DT–MR images instead of compute it directly from raw data as Tuch et al. in [9, 10, 11]. In our method, the capture time for the DT–MR images is not modified but the computational time.

2. The presented method is based on the minimization of a quadratic potential function. So that, the minima can easily be computed by gradient descent type methods or, as in our case, by a memory efficient Gauss–Seidel scheme. According to our experiments, the method is robust to the parameter set and the tensor basis selected.

3. The proposed multi–tensor restoration method can efficiently be used as a generic filtering method of tensor fields, as was demonstrated by experiments.

4. We presented a novel stochastic particle walk procedure based on Bayessian estimation theory and a second order Markov random process model. The procedure allow us to estimate the fiber pathways and therefore deduct the brain connectivity. The stochastic movement of the particle allows one to explore possible bifurcations on fiber bundles.

Acknowledgments

We thank to James C. Gee from the University of Pennsylvania who gently provided us the DT–MRI data used in the experiments. The code for the method reported in [15] was obtained from the library Web page provided for the au-

thors: *http://mscl.cit.nih.gov/spaj/dti/bcadt*. We thank to Arturo Hernandez for his comments that improved the quality of the paper.

References

[1] C.F. Westin, S.E. Maier, H. Mamata, F.A. Jolesz, R. Kikinis, "Processing and Visualization for Diffusion Tensor MRI," Medical Image Analysis, 6(2):93–108, 2002.

[2] C.F. Westin, S.E. Maier, B. Khidhir,P. Everett,F.A. Jolesz, R. Kikinis, "Image Processing for Diffusion Tensor Magnetic Resonance Imaging," In: Taylor C, Colchester A, editors. MICCAI 99, Sep 9–22, Cambridge, England. Heidelberg, Germany: Springer Verlag, 441–452, 1999.

[3] P.J. Basser and S. Pajevic and C. Pierpaoli and J. Duda and A. Aldroubi, "Microestructural and phisiological features of tissues elucidated by quantitative–diffusion–tensor MRI," J. Magn. Reson., 111, 209–219, 1996.

[4] P.J. Basser and S. Pajevic and C. Pierpaoli and J. Duda and A. Aldroubi, "In Vivo Fiber Tractography Using DT-MRI Data," Magn. Reson. Med.. 44 (2000) 625-632.

[5] O. Coulon, D.C. Alexander and S.R.Arridge. Tensor Field "Regularisation for DT-MR Images," Proc. MIUA'01, Medical Image Understanding and Analysis, Birmingham, United-Kingdom, 2001.

[6] M. Björnemo, B. Anders "White Matter Fiber Tracking Using Diffusion Tensor MRI," Master's Thesis, Linköping University, Reg nr: LiU-IMT-EX-321, 2002.

[7] D. C. Alexander, G. J. Barker, S. R. Arridge. Detection and "Modelling of non-Gaussianity in MR Diffusion Imaging Institute of Neurology," University College London, Dept. Comput. Science Research Note, RN/01/35, 2001.

[8] F. Vigueras, *Filtrado y segmentación de imágenes usando difusión anisotrópica*, Master's Thesis in Computer science and industrial mathematics, Centro de Investigacion en Matemáticas (CIMAT), México, 2001.

[9] D.S. Tuch, R.M. Weisskoff, J.W. Belliveau, V.J. Wedeen, "High angular resolution diffusion imaging of the human brain," Proc. 7th Annual Meeting of ISMRM, Philadelphia, 321, 1999.

[10] D.S. Tuch, T.G. Reese, M.R. Wiegell, N. Makris, J.W. Belliveau, Wedeen VJ. "High angular resolution diffusion imaging reveals intravoxel white matter fiber heterogeneity," Magnetic Resonance in Medicine, 48(4), 577, 2002

[11] D.S. Tuch, "Diffusion MRI of complex tissue structure," Doctoral Thesis, Harvard-MIT, Cambridge MA, 2002.

[12] S. Geman and D. Geman, "Stochastic relaxation, Gibbs distribution and the Bayesian restoration of images," IEEE Transactions on Pattern Analysis and Machine Intelligence, 6, 6, 721-741, 1984.

[13] S.Z. Li, *"Markov Random Field Modeling in Image Analysis,"* Springer Verlag, Tokyo, 2001.

[14] G.J.M. Parker, C.A.M. Wheeler-Kingshott, G. J. Barker, "Estimating Distributed Anatomical Brain Connectivity Using Fast Marching Methods and Diffusion Tensor Imaging," IEEE Transactions on Medical Imaging, 21, 5, 2002.

[15] S. Pajevic, A. Aldroubi, and P.J. Basserz. "A Continuous Tensor Field Approximation of Discrete DT-MRI Data for Extracting Microstructural and Architectural Features of Tissue," Journal of Magnetic Resonance, 154, 85100, 2002.

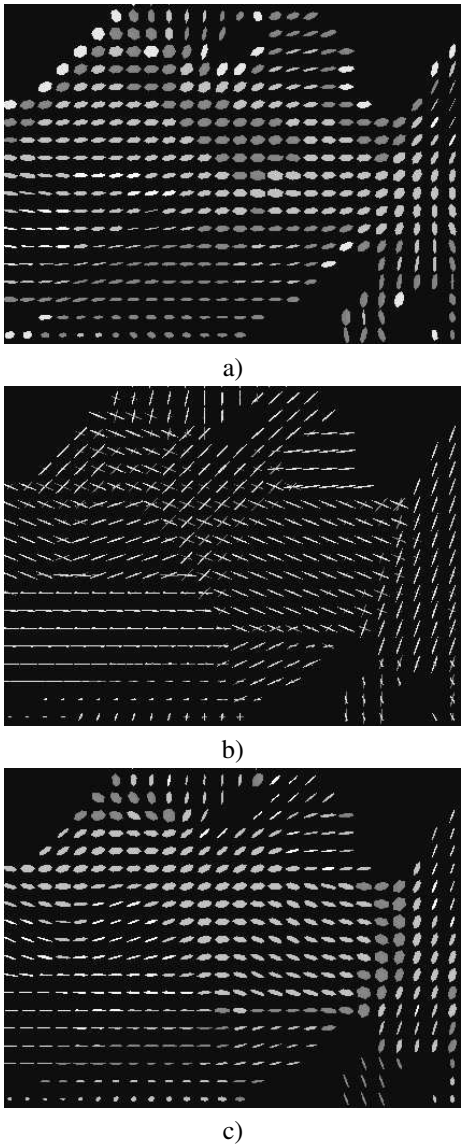

Figure 13: Filtering of tensor fields (a region of detail). a) DT–MRI input data. b) intra–voxel restoration and c) filtered tensor field (see text).

[16] B. C. Vemuri, Y. Chen, M.Rao, T.McGraw, Z. Wang and T.Mareci, "Fiber Tract Mapping from Diffusion Tensor MRI," IEEE Workshop on Variational and Level Set Methods (VLSM'01), 81, 2001.

[17] L. Zhukov and A.H. Barr, "Oriented Tensor Reconstruction: Tracing Neural Pathways from Diffusion Tensor MRI," Proceedings of IEEE Visualization 2002, 387-394, October 2002.

[18] Buxton Richard. Introduction to Functional Magnetic Resonance Imaging Principles and Techniques. Cambridge: Cambridge University Press; 2002.